Chapter 2

A Modified Slotted Patch Antenna with Defected Ground using Metasurface for Dual-band Applications

2.1. Introduction

Nowadays, metasurfaces (MS) take part in a major role due to the incorporation of cutting-edge methodologies, concepts, information, and design styles for a variety of microwave devices. [1-5]. These are manufactured as a periodic group of conducting elements such as metallic rings, rods, or various geometrical shapes that form electromagnetic mediums simultaneously, and the resonant effects of the MS are controlled by the geometry of the unit cells [6-14]. Furthermore, the use of fractal geometrical patterns reduces the electrical length of the device, making it much more compact [116-118]. The iteration number and iteration factors of square-shaped fractal increase the resonance frequencies of the structure and become more efficient than the original one [116-118]. A slotted patch antenna with fractal geometry and a periodic MS at the bottom of the substrate along with the partial ground is a relatively new technique that allows for simultaneous operation at a higher frequency range while maintaining antenna miniaturization. [119-121]. The defective ground structure

suppresses the surface wave, hence lowering cross-polarized radiation [122]. The slot in the patch of the radiating antenna has also been used to enhance the co- to cross-polarized radiation characteristics in the broadside direction, having wide impedance bandwidth [123]. MS in the ground plane suppresses the generation of surface waves and thereby reduces the size of the antenna by using the same dielectric [124-125].

A novel, modified, compact, dual, and wideband MS-based antenna with high gain is proposed in this chapter. The realization of bandwidth improvement of the antenna is extremely difficult using a conventional microstrip patch having a compact dimension. However, the introduction of MS in the ground plane provides enhancement of bandwidth as well as gain to a large extent maintaining the original compactness. The proposed antenna comprises a fractal-shaped slotted patch above the dielectric and a 4×5 periodic MS at the bottom of the dielectric with the partial ground. The MS has been designed by a periodic combination of two L-type patches with cantered C-type shaped patch. The proposed antenna has been simulated in Ansys HFSS [126] and the final structure offers very good impedance matching at both bands. Initially, a simple conventional modified square-shaped fractal patch design makes the gain enhanced to 5.3 dBi along with a bandwidth of 322 MHz at 10.54 GHz operating frequency. However, the introduction of MS at the bottom of the dielectric substrate enhances the realized gain of the antenna to 7.16 dBi. Furthermore, the designed prototype operates in two frequency bands viz., 1.80-5.70 GHz and 10.38-10.92 GHz. Nearly Omni-directional radiation characteristics have been noticed from 1.80 GHz to 5.70 GHz while similar characteristics are seen in the higher band with few degrees of degradation in radiation near 0-30^{o} elevation. The designed prototype has been fabricated and experimental characterization of the antenna has been carried out. The simulated and experimental results are found to be in close agreement with each other.

2.2. Design and Analysis

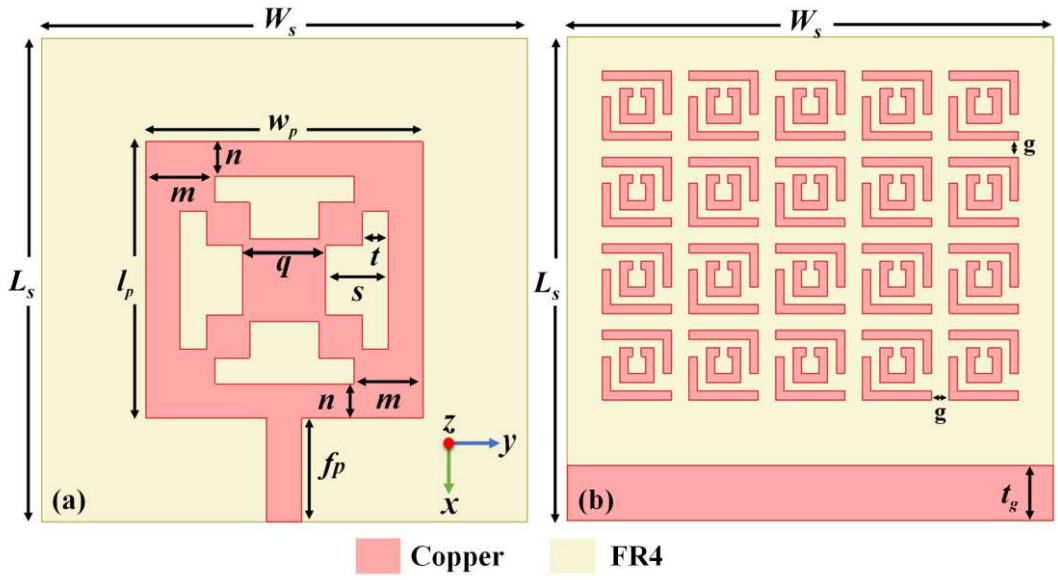

Fig. 2.1. (a) Top and (b) bottom views of the proposed antenna (Designed parameters: W_s = 28 mm, L_s = 28 mm, w_p = 16 mm, l_p = 16 mm, m = 4 mm, n = 2 mm, q = 4.8 mm, s = 3.6 mm, t = 1.5 mm, f_p = 6 mm, g = 1 mm, t_g = 3.2 mm).

The proposed antenna consists of a square fractal patch on a simple microstrip antenna where a 4×5 order MS has been introduced just opposite to the patch. The partially ground plane [127-129] and MS lie on the same plane in which the MS consists of a combination of two L-type patches at the outer of the unit cell along with a centered C-type patch. Here the unit cells are arranged in such a way that it obeys the homogeneity properties of metamaterial [16-17]. The periodic arrangement of symmetric metallic unit cells creates a class of subwavelength particles that exhibit a strong resonance response to the applied electric field and negligible response to the magnetic field. Due to this reason, it enhances the bandwidth of the antenna as well as gain. The single-layer slotted patch antenna with MS is propagating

in TM_{01} mode. Here, the TM_{01} excitation is highest with the least power coupling at a specified feed position.

The top and bottom views of the proposed antenna structure are shown in Figs. 2.1(a) and 2.1(b) respectively. All the optimized geometrical dimensions are also mentioned in Fig. 2.1. The modified fractal shape has been designed on FR-4 dielectric (relative permittivity of 4.4 and loss tangent of 0.025) with a thickness of 1.6 mm. Copper has been used as metallic patches on both top and bottom surfaces. The designed antenna has been evolved by using five steps as graphically represented in Fig. 2.2. For the purpose of the design analysis, the reflection characteristics of each step have been mentioned in Fig. 2.3.

2.2.1. Design of the Microstrip Slotted Patch

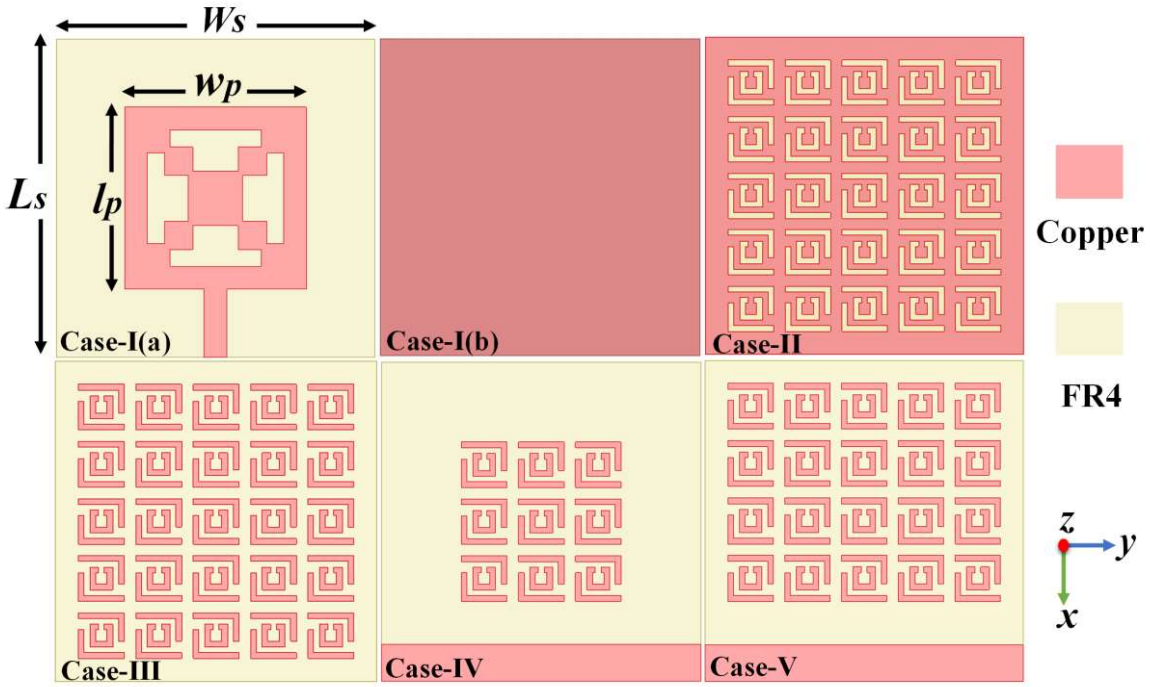

Fig. 2.2. Design evolution for the proposed structure with different modifications.

Initially, a simple rectangular microstrip patch with a 1.6 mm thick FR4 substrate has been used to start the design analysis of the conventional patch. A profile closer to half wavelength

has been selected based on the operating frequency. The patch dimensions w_p and l_p are tuned for required resonant frequencies. Since the microstrip patch is limited by its narrow bandwidth and low gain, it has been modified to a fractal one in order to increase impedance bandwidth; thereby improving the performance. Here, the fractal-shaped slots have been introduced on the original patch antenna as illustrated by Case-I of Fig. 2.2. Four distinct fractal square-shaped slots have been formed by etching in the patch. The single-layer slotted patch antenna with MS is propagating in TM_{01} mode. Here, the TM_{01} excitation is highest with the least power coupling at a specified feed position. The patch is fed at a distance of λ/4 from the centre of the non-radiating edge for good impedance matching. The top and bottom views of the radiating patch have been shown in Case-I of Fig. 2.2(a) and Fig. 2.2(b) respectively.

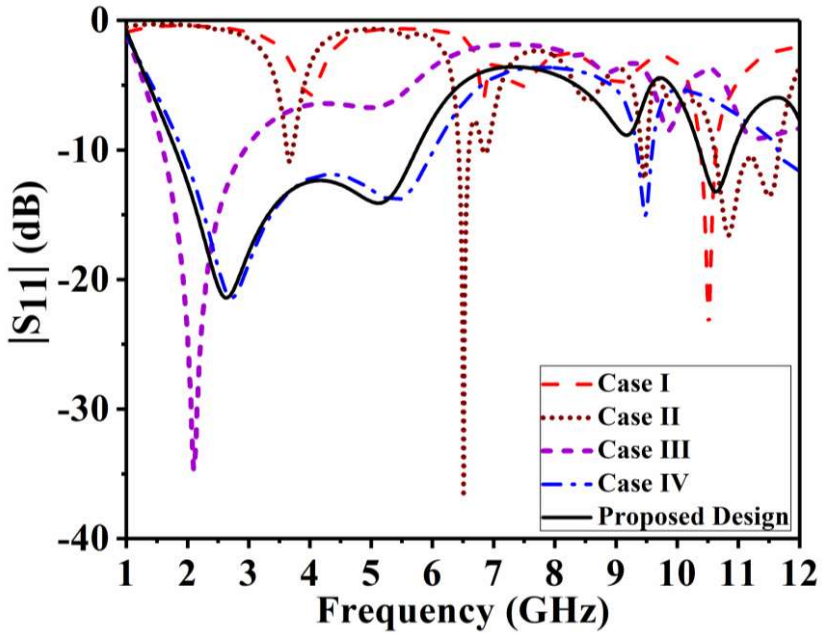

Fig. 2.3. The plot of $|S_{11}|$ (dB) with respect to frequency (GHz) for different variations of the antenna is mentioned in Fig. 2.2, along with the proposed antenna.

Table 2.1. Effect of Slot Loading on the Patch with Different Iteration

Iteration No.	Prototype	Resonant Frequency (GHz)	Bandwidth (MHz)	Z-parameter (Ω)
1	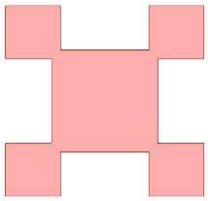	11.75	330	51.3 + j3.67
2	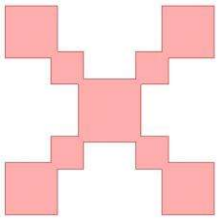	10.54	322	56.56 + j1.03

The effect of loading of the slots has been studied by change of the fractal order as listed in Table 2.1. It has been observed that the increase of fractal iteration enables improved impedance matching. Furthermore, the integration of the modified square-shaped fractal design to the simple patch increases the impedance bandwidth to 322 MHz and the gain to 5.3 dBi at the operating frequency of 10.54 GHz. The impedance bandwidth and gain are both improved to a certain extent. This is the fundamental mode of the operating frequency of this antenna.

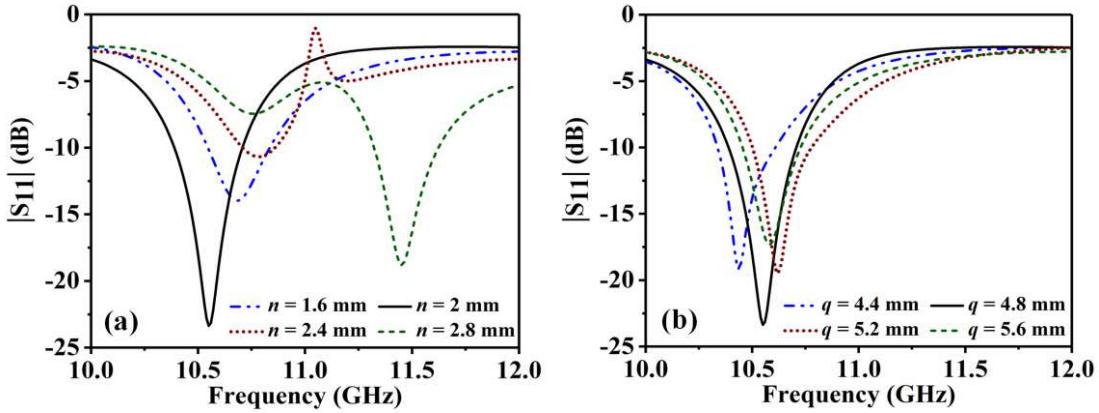

Fig. 2.4. Plot of $|S_{11}|$ (dB) with respect to frequency (a) at constant *n* variations (b) at constant *q* variations.

The parametric variation of the outer patch interface (n) and the centre patch width (q) have been studied in Fig. 2.4. It has been observed that at n = 2 mm and q = 4.8 mm the patch maintains good reflection characteristics with respect to frequency. For the higher values of n and q, the reflection characteristics are not properly maintained.

2.2.2. Unit Cell in the Ground Plane of Rectangular Fractal Patch

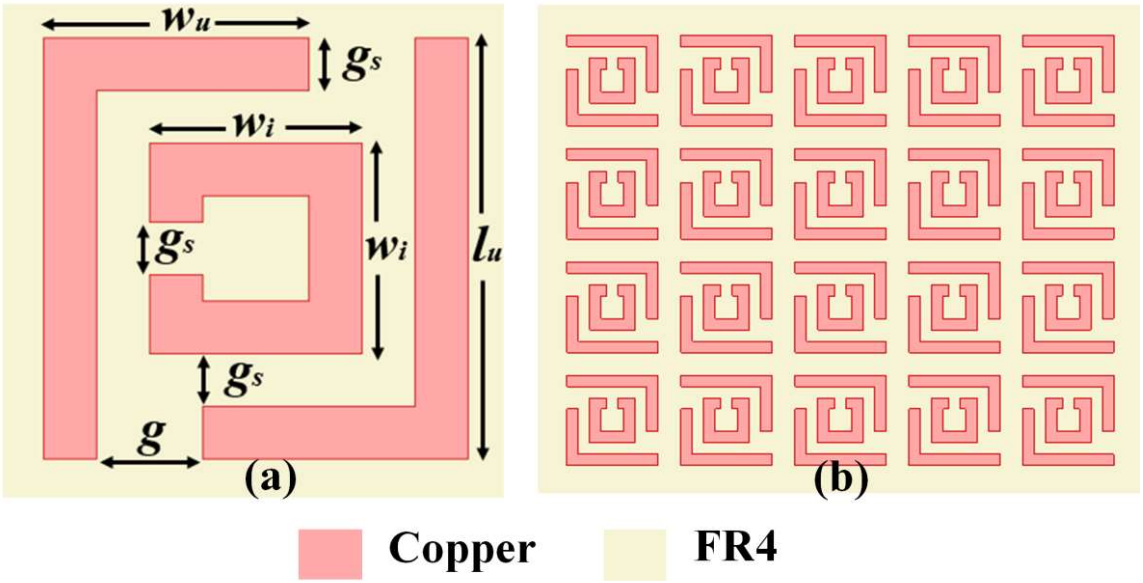

Fig. 2.5. (a) The bottom view of the unit cell of the defected ground structure for the proposed antenna (Designed parameters: l_u= 4 mm, w_i= 2 mm, w_u = 2.5 mm, g = 1 mm, g_s = 0.5 mm) along with (b) 4×5 unit cells in the ground plane.

In this design, represented as Case-II and Case-V in Fig. 2.2, MS designs are incorporated in the ground plane. A unit cell consisting of two L-type patches in the outer side along with a centered C-type patch is made along the axis of the resonating length. All the optimized geometrical dimensions of the proposed unit cell are mentioned in Fig. 2.5(a) and the proposed 4×5 order MS is illustrated in Fig. 2.5(b). The reflection and transmission characteristics of 4×5 order MS with respect to frequency has been depicted in Fig. 2.6 and

it is evident from Fig. 2.6 that the aforementioned MS provides transmission minima at 5.1 GHz, 8.56 GHz, and 11.20 GHz with fractional bandwidths of 13.1%, 1.1%, and 0.08% respectively. In Case-II, a 5×5 order unit cells are arranged in a complementary manner. When the periodic cells are arranged in 3×3 order in a complementary manner the antenna operates at three different frequencies 6.54 GHz, 9.59 GHz, and 10.22 GHz with respective fractional bandwidths of 1.95%, 0.42%, and 1.84%. By increasing the order to 5×5 periodic unit cell slots in the ground plane, the antenna operates over six distinct frequencies viz., 3.68 GHz, 6.51 GHz, 6.87 GHz, 9.47 GHz, 10.75 GHz, and 11.37 GHz with respective fractional bandwidths of 3.26%, 2.76%, 1.74%, 1.05%, 3.16%, and 5.1% while the maximum realized gain of 11.10 dBi is achieved at 11.37 GHz.

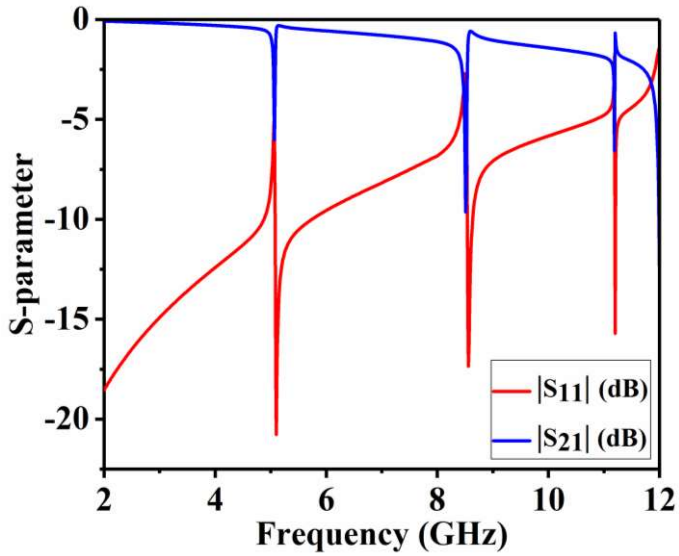

Fig. 2.6. The plot of reflection and transmission characteristics of MS with respect to frequency (GHz).

From this, it is clearly observed that the rise in the number of complementary unit cells in the ground plane increases the different resonating frequencies due to more inductive and capacitive effects [66-67]. But more number of different resonating frequencies are less effective compared to a wider bandwidth. So 5×5 order unit cells are directly imposed on the

ground plane due to this 72% fractional bandwidth with 0.14 dBi realized gain is observed at 2.02 GHz frequency. It enhances the bandwidth as compared to the previous one and also shifts the operating frequency to a lower value.

2.2.3. Unit Cell along with Partial Ground of Rectangular Fractal Patch

In Case-III, the 5×5 order unit cells are directly incorporated in the ground plane. Later 3×3 and 4×5 periodic unit cells along with partial ground are placed which are depicted as Case-IV and Case-V of Fig. 2.2. The gap between the two opposite faces of the L-shaped patch and C-shaped patch is varied around the axis of the resonating length of the rectangular patch.

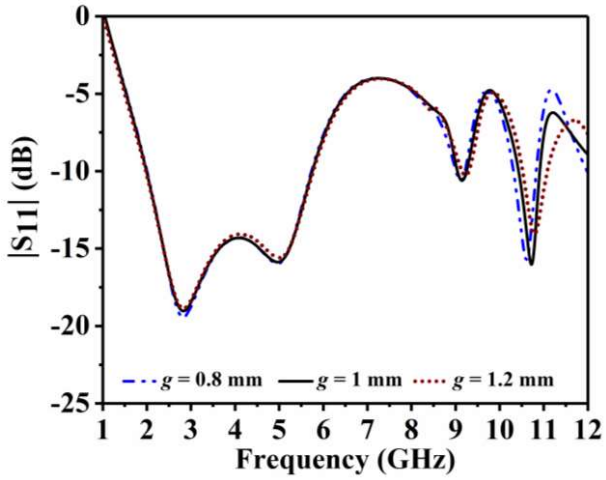

Fig. 2.7. The plot of $|S_{11}|$ (dB) with respect to frequency for *g*-variations.

The periodic 3×3 order unit cells arranged in this antenna operate in enhanced bandwidth ranging from frequencies 1.91 GHz to 6.02 GHz and 9.35 GHz to 9.59 GHz with fractional bandwidths of 150% and 2.5% respectively at 2.73 GHz and 9.47 GHz. In this case, the impedance bandwidth is increased while the gain undergoes reduction. Moreover, the radiation pattern is not very good. For this purpose, a 4×5 order unit cells have been used which maintain the bandwidth identical to the first band with the previous case but it enhances the second band with a good radiation pattern. This antenna has been studied by

varying different gap lengths and widths of unit cells along with the thickness of the ground plane. The parametric variation of the unit cell gap (g) has been mentioned in Fig. 2.7. Figure 2.8 depicts the parametric variation of partial ground thickness (t_g) with respect to frequency. The impedance bandwidth improves when the width is increased to t_g = 3.2 mm. When the width of the ground plane is lowered, the operating bands become narrower; however, when the width of the ground plane reaches a certain limit, the impedance band becomes wider.

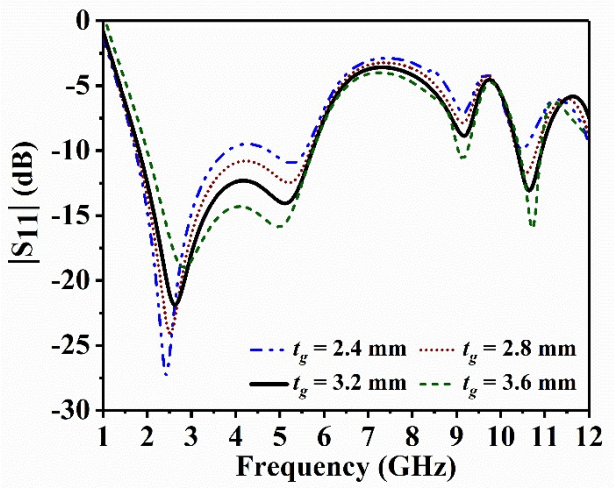

Fig. 2.8. The plot of $|S_{11}|$ (dB) with respect to frequency for t_g -variations.

The antenna operates over the dual-frequency ranges viz., 1.80-5.70 GHz and 10.38-10.94 GHz with fractional bandwidths of 150% and 5.09% at 2.6 GHz and 10.6 GHz respectively. The maximum realized gain of 7.16 dBi has been achieved at 10.6 GHz. This Case-V of Fig. 2 is the final design of the proposed antenna due to improved performance.

2.3. Simulated Results

The respective return loss characteristics of the conventional patch antenna and the proposed design with respect to the frequency are shown in Fig. 2.9. The conventional antenna operates at 10.54 GHz and has a -10 dB impedance bandwidth of 3.02 %, making it a narrowband

antenna. The proposed antenna operates over two wideband frequencies ranging from 1.8 GHz to 5.7 GHz and 10.38 GHz to 10.92 GHz with fractional bandwidths of 150% and 5.09% at 2.6 GHz and 10.6 GHz as observed from Fig. 2.9. The maximum return loss of 21 dB has been achieved over the frequency band of 1.80-5.70 GHz at 2.6 GHz.

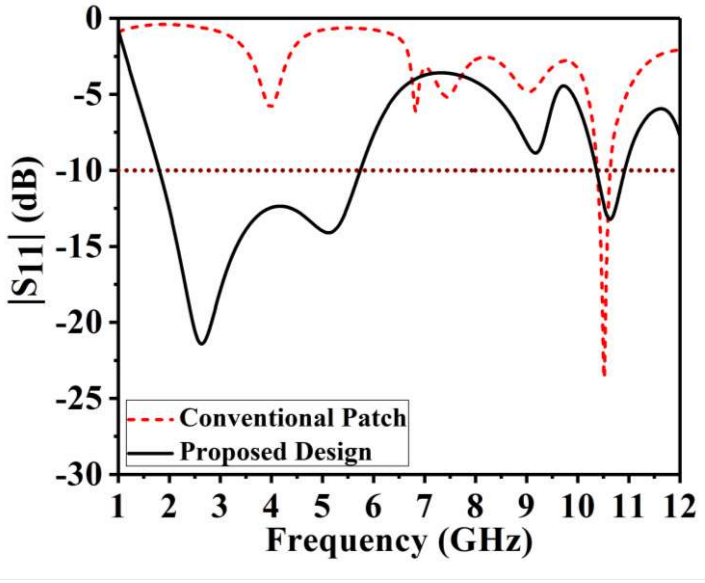

Fig. 2.9. The plot of $|S_{11}|$ (dB) with respect to frequency (GHz) for conventional patch antenna along with the proposed one.

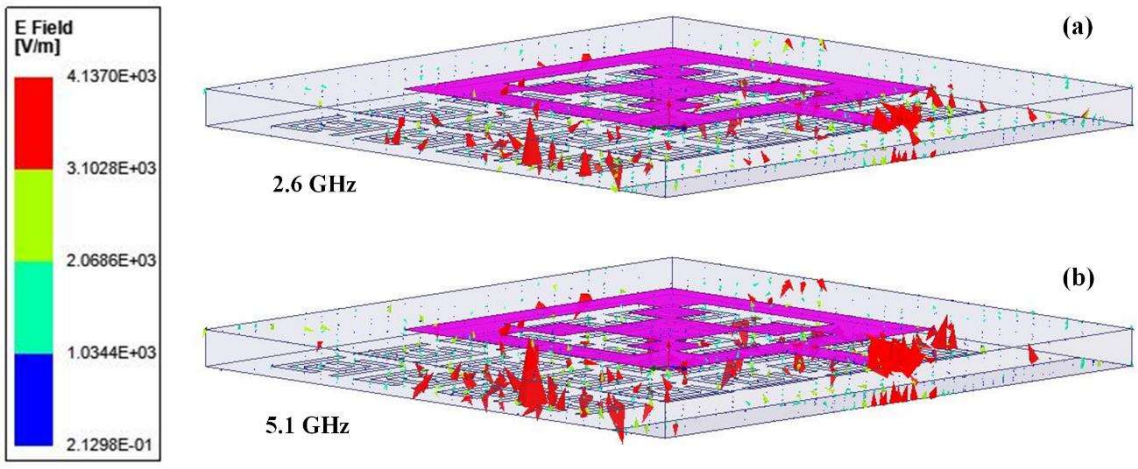

Fig. 2.10. Electric field distributions of the proposed antenna at (a) 2.6 GHz and (b) 5.1 GHz.

The introduction of a gap between two L-type patches on the outer side and a centred C-type patch generates equivalent mutual capacitance within the unit cell, hence lowering the operating frequency. Finally, the incorporation of 4×5 order metasurface in the ground surface, significantly improves the impedance matching and the narrow bandwidth; yielding excellent broadband characteristics in the lower band.

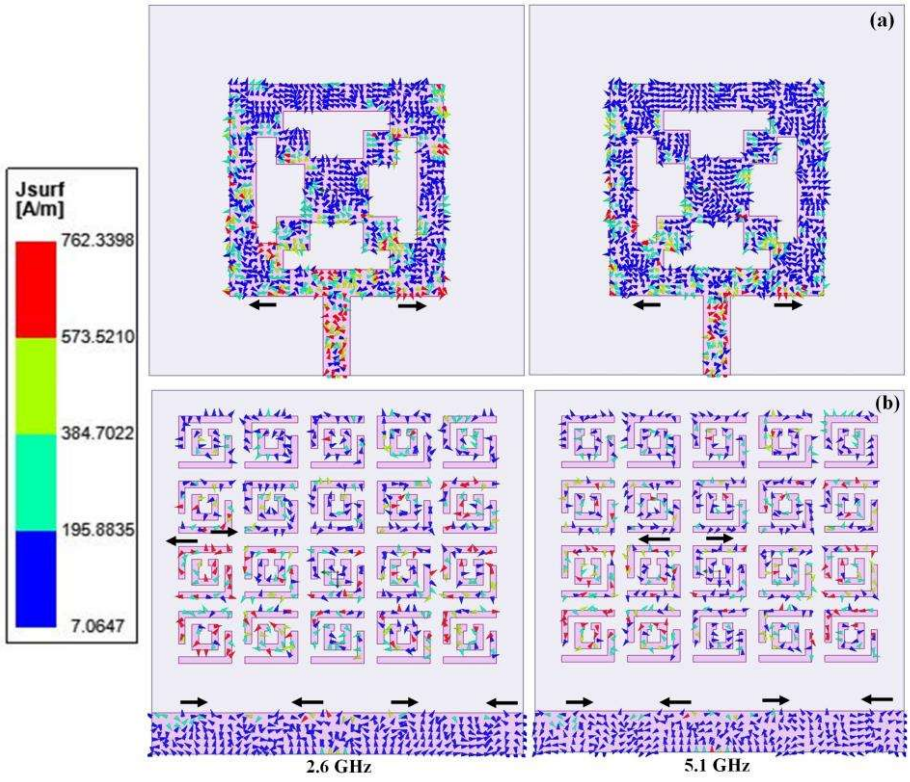

Fig. 2.11. Surface current distributions at (a) top and (b) bottom surfaces at 2.6 GHz and 5.1 GHz.

The normalized electric field distributions of the prototype at different operating frequencies are depicted in Fig. 2.10. The physical working mechanism of antenna structures is easily understood with the help of electric field and magnetic field distribution diagrams. The vector plots of the same provide the direction of the radiation of the antenna structures. The field distribution is maximum along the edge of the antenna. The maximum field distribution along

the length of the unit cell slots has been observed due to the incorporation of inductive and capacitive effects [66-67]. Next, the surface current distributions of the squared shape fractal slot and periodic unit cells in the bottom surface are studied and subsequently illustrated in Fig. 2.11(a) and Fig. 2.11(b) respectively. There is an optimum coupling current both the radiating patch and the MS at 2.6 GHz and 5.1 GHz. They are intense around the antenna interface and the slot portion of the unit cell.

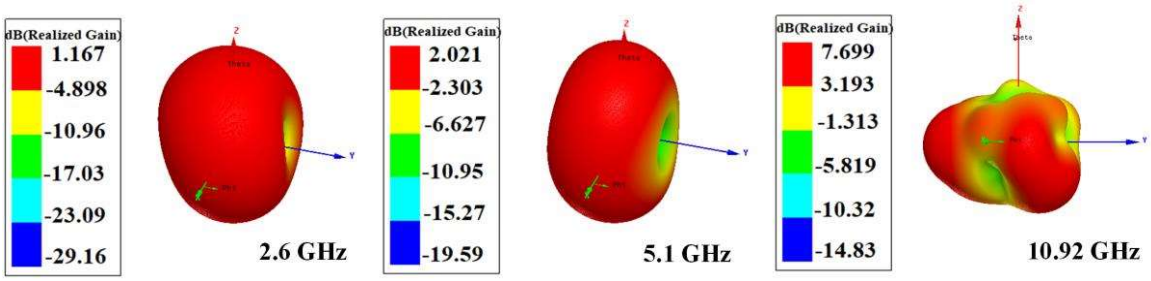

Fig. 2.12. 3D Polar Plot at different operating frequencies within the proposed antenna.

The three-dimensional polar plots at 2.6 GHz, 5.1 GHz and 10.92 GHz are shown in Fig. 2.12. The reasonable gain is achieved over the entire band and the maximum gain of 7.69 dBi has been achieved at 10.92 GHz. The realized gain of the antenna undergoes modification over different operating frequencies due to the incorporation of more slots in the patch as well as in MS. Besides gain, the patterns are giving information about radiation characteristics such as the behaviour of radiation, side-lobe level, back-lobe, etc.

2.4. Experimental Results

The experimental study of the proposed prototype, including its reflection and radiation characteristics, is shown in Fig. 2.13. The antenna prototype has been fabricated using LPKF PCB Prototyping Instrument [130]. The top and bottom views of the fabricated structure are depicted in Fig. 2.13(a) and Fig. 2.13(b) respectively. The fabricated prototype is connected

to one of the ports of Vector Network Analyzer (VNA) Anritsu, model MS 2037C as shown in Fig. 2.13(c).

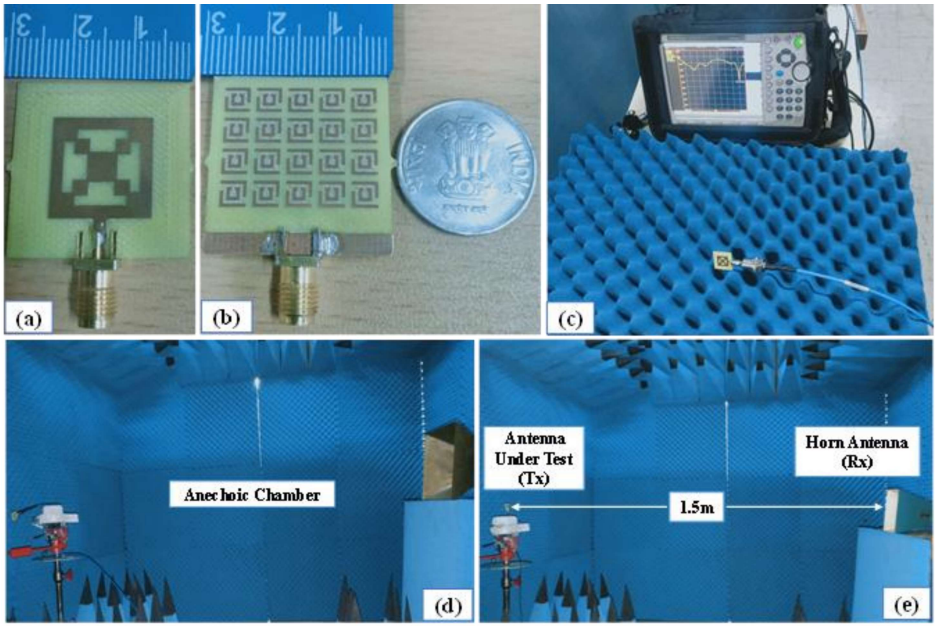

Fig. 2.13. Proposed fabricated structure: (a) top view, (b) bottom view, (c) $|S_{11}|$ measurement using VNA, (d) E-plane radiation pattern measurement and (e) H-plane radiation pattern measurement within the anechoic chamber.

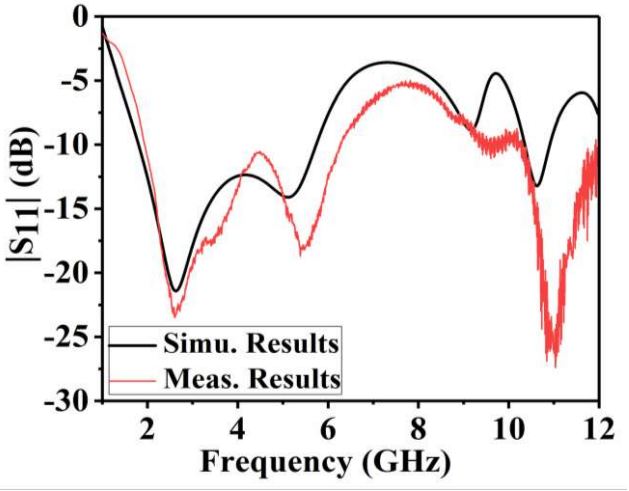

Fig. 2.14. The plot of simulated and measured return losses with respect to frequency of the proposed antenna.

The return loss profile of the fabricated antenna has been measured and shown in Fig. 2.14 where it is compared with the simulated one. The antenna operates over the bandwidths 1.93 GHz-6.62 GHz and 10.32 GHz-11.90 GHz as depicted from Fig. 2.14. The comparison of simulated and experimental return loss profiles of the proposed antenna is shown in Table 2.2. A small shift in the higher band of the experimental results has been observed which can be attributed to the fabrication tolerances and other experimental errors.

Table 2.2. Comparison of Simulated Results with Measured Results of the Proposed Antenna

Results	Frequency (GHz)		Return Loss (dB)	
	BW I	BW II	BW I	BW II
Simulated	1.8-5.7	10.38-10.92	21	13
Measured	1.93-6.26	10.32-11.90	22	26

Then E-plane radiation pattern measurement and H-plane radiation pattern measurement of the antenna have been carried out within an anechoic chamber as represented in Fig. 2.13(d) and Fig. 2.13(e) respectively. Three distinct horn antennas covering s-band, c-band, and X-band have been used to characterize the test antenna. The far-field distance between the test antenna and reference antenna is clearly indicated as 1.5m in Fig. 2.13(e) implying that the antenna under test has been kept in the far-field region. The E-plane ($\varphi = 0^0$) and H-plane ($\varphi = 90^0$) radiation characteristics of the proposed antenna have been studied and shown in Fig. 2.15(a) and Fig. 2.15(b) respectively. Nearly omnidirectional radiation characteristics are noticed at 2.60 GHz and 5.10 GHz along the E-plane. The cross-pol levels of both E and H-planes are reduced whereas the co-pol levels offer large value at a few frequencies due to the metasurface placed just opposite side of the top patch along with the partial ground.

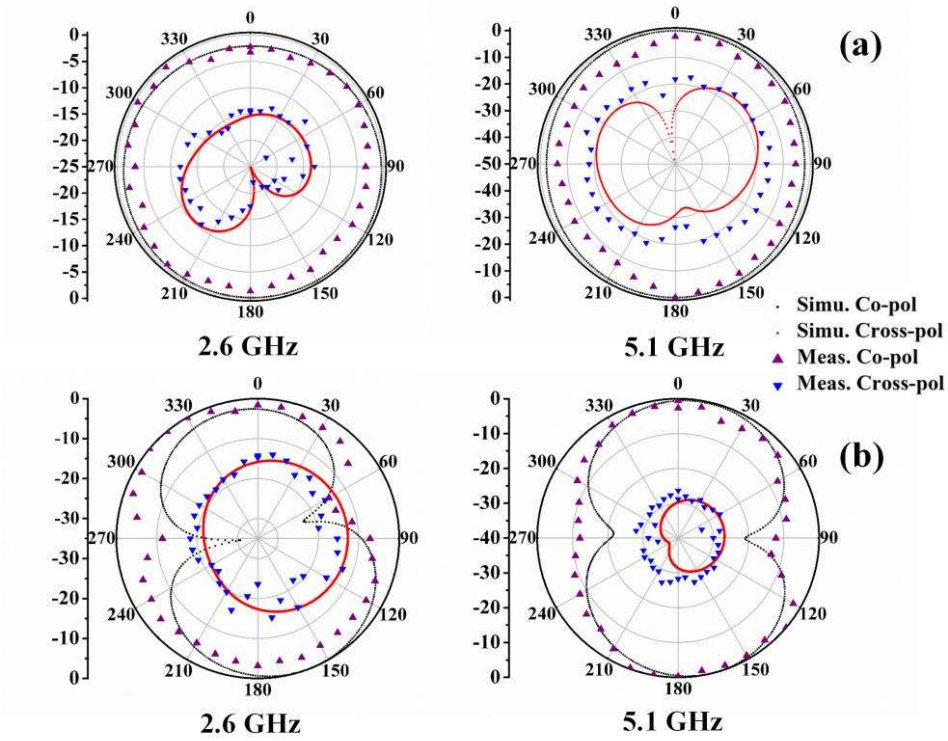

Fig. 2.15. Co-polarized and Cross-polarized (a) E-plane and (b) H-plane radiation patterns at different operating frequencies of the proposed antenna structure.

The cross-polarized level is found to be 15 dB below the co-polarized level at all the operating frequencies. It is seen that at the lower frequency the antenna exhibits a good omnidirectional pattern. On the contrary, at the higher frequency, slight degradation in the radiation profile is noted. Nevertheless, it may be observed from Fig. 2.15 that, still the radiation pattern is nearly omnidirectional at such high frequency with few degrees of degradation in radiation near 0-30^{o} elevation. This may be due to leakage of out of phase fields from few slots either in the ground plane or at the patch. However, such distortion at high frequency is still acceptable for wireless handheld devices working in the multipath environment. In this experiment, there are some discrepancies between the measured and simulated results due to fabrication precision, dielectric loss, cable, and adaptor losses during the far-field measurement system.

Table 2.3. Comparison of the Proposed Antenna with Existing Metasurface Based Antennas

Antenna Literature	**Dimension (mm^2)**	**Operating Frequency (GHz)**	**Fractional BW (%)**	**Gain (dBi)**
Cai et. al. [110]	40×45 ($0.47\lambda_0 \times 0.74\lambda_0$)	3.5	3.7	4.9
Zhai et. al. [114]	104×104 ($0.83\lambda_0 \times 0.83\lambda_0$)	2.4, 5.2	15.6, 9.3	7.2, 7.3
Nasser et. al. [131]	80×80 ($1.5\lambda_0 \times 1.5\lambda_0$)	5.62	33.6	8.5
Xu et. al. [132]	88×88 ($0.22\lambda_0 \times 0.22\lambda_0$)	0.72, 0.79, 0.92	2.3, 0.8, 18	3.7, 2, 4.8
Alibakhshi-Kenari et. al. [133]	40×35 ($0.36\lambda_0 \times 0.36\lambda_0$)	2.76	165.84	4.45
Li et. al. [134]	32×28 ($0.82\lambda_0 \times 0.71\lambda_0$)	7.7	46.37	7.2
Mitra et. al. [135]	60×60 ($1.72\lambda_0 \times 1.73\lambda_0$)	8.66	10.74	4.5
Li et. al. [136]	63×108 ($0.78\lambda_0 \times 1.35\lambda_0$)	3.75	101.3	7.32
Huang et. al. [137]	39.2×40 ($0.73\lambda_0 \times 1.74\lambda_0$)	5.6	32	7.8
Zhu et. al. [138]	120×120 ($0.92\lambda_0 \times 0.92\lambda_0$)	2.3, 2.6	15.5, 17.6	5.8
Nasimuddin et. al. [139]	60×88 ($0.8\lambda_0 \times 1.17\lambda_0$)	4	34.56	7.4
Xu et. al. [140]	43.5×43.5 ($0.45\lambda_0 \times 0.45\lambda_0$)	3.11	1.61	4.15
Proposed Design	**28×28 ($0.24\lambda_0 \times 0.24\lambda_0$)**	**2.6, 10.6**	**150, 5.09**	**1.91, 7.16**

The proposed structure has been compared with a few existing reported MS-based antenna structures as shown in Table 2.3. It is observed that the proposed design offers compact

dimensions with optimum bandwidth and significantly enhanced gain in comparison with the reported ones.

2.5. Concluding Remarks

The rectangular fractal shape slotted patch antenna has been analyzed by using a 4×5 order periodic MS. It has been observed that bandwidth and gain are more affected due to partial ground along with the arrangement of unit cells. Good impedance matching in dual-band region is achieved by using the concept of fractal and the use of 4×5 periodic two L-type shaped patches with centered C-type patch unit cell. The proposed antenna operates at two different operating frequencies 2.6 GHz and 10.60 GHz with respective fractional bandwidths of 150% and 5.09% exhibiting dual-band operation and significantly enhanced gain of 7.16 dBi at 10.92 GHz. The antenna exhibits an almost omnidirectional radiation pattern from 1.8 GHz to 5.7 GHz and a unidirectional radiation pattern from 10.38 GHz to 10.92 GHz in its far-field characteristics. The MSA has been fabricated and measured in order to validate the accuracy of the simulation results. The results of the simulation and the experiments are very close to each other. The designed antenna can find its application towards WLAN, mobile, radio astronomy, and microimaging in medical analysis.